Quantum phase transition in Hall conductivity on an anisotropic kagome lattice

Shun-Li Yu, Jian-Xin Li,* and Li Sheng
National Laboratory of Solid State Microstructures and Department of Physics, Nanjing University, Nanjing 210093, People's Republic of China

(Received 31 July 2009; revised manuscript received 10 October 2009; published 5 November 2009)

We study theoretically the quantum Hall effect (QHE) on the kagome lattice with anisotropy in one of the hopping integrals. We find an interesting quantum phase, in which the QHE exhibits the energy spectrum given by $E(n)=\pm v_F\sqrt{(n+1/2)\hbar Be}$ (n is an integer) being different from the known types, though its quantization rule for Hall conductivity $\sigma_{xy}=2ne^2/h$ is conventional. This phase evolves from the QHE phase with $\sigma_{xy}=4(n+1/2)e^2/h$ and $E(n)=\pm v_F\sqrt{2n\hbar Be}$ in the isotropic case, which is realized in a system with massless Dirac fermions (such as in graphene). The phase transition does not occur simultaneously in all Hall plateaus but occurs in a sequence from low to high energies, with the increase in hopping anisotropy.

DOI: 10.1103/PhysRevB.80.193304 PACS number(s): 73.43.Cd, 73.43.Nq, 71.70.Di

The quantum Hall effect (QHE) is a remarkable transport phenomenon in condensed-matter physics.[1] Up to know, three known kinds of integer QHE have been found in materials. One is the conventional integer QHE occurring in two-dimensional (2D) semiconductor systems, where the successive filling of the Landau levels (LLs) leads to an equidistant ladder of quantum Hall plateaus at integer filling $n=0,\pm 1,\pm 2,\cdots$, with a quantized value $\sigma_{xy}=2ne^2/h$.[1] The second is the unconventional QHE observed in graphene, where charge carriers mimic the massless Dirac fermions, so that the Hall conductivity is half-integer quantized $\sigma_{xy}=4(n+1/2)e^2/h$ due to a Berry phase shift π at the Dirac points.[2–8] The third occurs in bilayer graphene, where the charge carriers have a parabolic energy spectrum but are chiral with a Berry's phase 2π. Therefore, the Hall conductivity follows the same ladder as in conventional 2D electron gases, but the plateau at zero level is absent.[9,10]

In this Brief Report, we demonstrate a topological quantum phase transition from an unconventional QHE for the massless Dirac fermions to a conventional one but with a special-energy spectrum. The kagome lattice has recently attracted considerable interest due to its higher degree of frustration. It is the line graph of the honeycomb structure in view of the graph theory.[11] The three-band electronic structure (Fig. 1) is composed of one flat band and two dispersive bands. The latter has the same form as that in graphene,[4] and the two bands touch at two inequivalent Dirac points forming massless Dirac fermions. As a result, an unconventional QHE with $\sigma_{xy}=4(n+1/2)e^2/h$ will be realized on the isotropic kagome lattice. Assuming one of the three hopping integrals, which is denoted by t_{23}, can take a different value from the two others, we find a quantum phase transition for the Hall conductivity from the unconventional form $\sigma_{xy}=4(n+1/2)e^2/h$ to $\sigma_{xy}=2ne^2/h$. Though the latter phase shows the same Hall conductivity as that found in conventional 2D semiconductors (free-fermion systems), it has the following nontrivial properties. (i) The phase is characterized by a special-energy spectrum $E(n)=v_F\sqrt{(n+1/2)\hbar Be}$, in contrast to $E(n)=(n+1/2)\hbar\omega_c$ with $\omega_c=eB/m$ for the free-fermion QHE systems, $E(n)=v_F\sqrt{2n\hbar Be}$ for the single-layer graphene[8] and $E(n)=\sqrt{n(n-1)}\hbar\omega_c$ for the bilayer graphene.[9,10] (ii) The quantum phase transition does not occur simultaneously in all Hall plateaus as expected usually but occurs in sequence from low to high energies with the increase in anisotropy. (iii) The quantum phase transition occurs only in the case of $t_{23}<t_{12}$ ($t_{12}=t_{13}$). In the other case of $t_{23}>t_{12}$, the unconventional QHE realized in the isotropic system remains at least for the largest anisotropy we considered here, namely $t_{23}=2t_{12}$. This kind of quantum phase structures controlled by the anisotropy of the hopping parameters is also in stark contrast to that in the honeycomb lattice (graphene), where the unconventional QHE evolves into the conventional one in the strong t_{23} ($t_{23}>t_{12}$) regime, while no phase transition occurs in the weak t_{23} ($t_{23}<t_{12}$) regime.[12–15] Therefore, the quantum phase transition demonstrated here presents an intriguing case for experimental studies on QHE. We start from the tight-binding model on a 2D metallic kagome lattice,

$$\hat{H}=-\sum_{\langle ij\rangle,\sigma}(t_{ij}\hat{c}^{\dagger}_{i\sigma}\hat{c}_{j\sigma}+\text{H.C.}), \tag{1}$$

where $\hat{c}_{i\sigma}$ ($\hat{c}^{\dagger}_{i\sigma}$) annihilates (creates) an electron with spin σ ($\sigma=\uparrow,\downarrow$) on site i and t_{ij} is the hopping integral between the nearest neighbors (NNs). Considering that there are three sites in each unit cell [see Fig. 1(a)], we can write Eq. (1) in the momentum space as $\hat{H}=\Sigma_{\mathbf{k}\sigma}\hat{\Psi}^{\dagger}_{\mathbf{k}\sigma}M(\mathbf{k})\hat{\Psi}_{\mathbf{k}\sigma}$. Where $\hat{\Psi}_{\sigma}(\mathbf{k})=(\hat{c}_{\mathbf{k}1\sigma},\hat{c}_{\mathbf{k}2\sigma},\hat{c}_{\mathbf{k}3\sigma})$, and $M(\mathbf{k})$ is a 3×3 matrix

$$M(\mathbf{k})=\begin{pmatrix}0 & \varepsilon_{12}(\mathbf{k}) & \varepsilon_{13}(\mathbf{k})\\ \varepsilon_{21}(\mathbf{k}) & 0 & \varepsilon_{23}(\mathbf{k})\\ \varepsilon_{31}(\mathbf{k}) & \varepsilon_{32}(\mathbf{k}) & 0\end{pmatrix}, \tag{2}$$

with $\varepsilon_{12}(\mathbf{k})=\varepsilon_{21}(\mathbf{k})=-2t_{12}\cos(\mathbf{k}\cdot\delta_1)$, $\varepsilon_{13}(\mathbf{k})=\varepsilon_{31}(\mathbf{k})=-2t_{31}\cos(\mathbf{k}\cdot\delta_3)$, and $\varepsilon_{23}(\mathbf{k})=\varepsilon_{32}(\mathbf{k})=-2t_{23}\cos(\mathbf{k}\cdot\delta_2)$. δ_1, δ_2, and δ_3 are the nearest-neighbor vectors, $\delta_1=(1/2)\hat{x}$, $\delta_2=(1/4)\hat{x}+(\sqrt{3}/4)\hat{y}$, and $\delta_3=-(1/4)\hat{x}+(\sqrt{3}/4)\hat{y}$. For the isotropic case ($t_{12}=t_{23}=t_{31}=t$), the energy bands are,

$$E_{\pm}(\mathbf{k})=-t\pm t\sqrt{1+f(\mathbf{k})},\quad E_3(\mathbf{k})=2t, \tag{3}$$

where

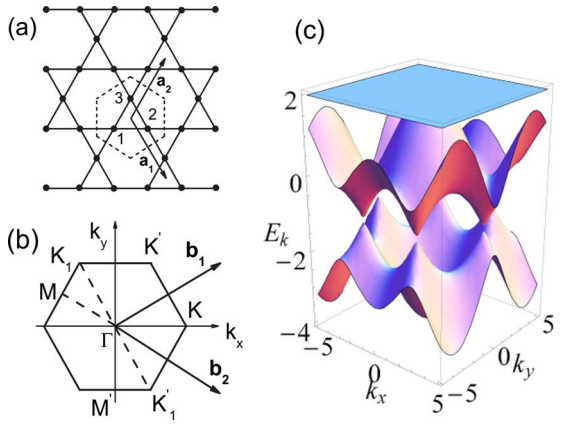

FIG. 1. (Color online) (a) Lattice structure of the kagome lattice. The region enclosed by the dashed lines represents the Wigner-Seitz unit cell. $\mathbf{a}_1$ and $\mathbf{a}_2$ are the lattice unit vectors. The lattice sites in each unit cell are labeled as 1, 2, and 3. (b) The first BZ. $\mathbf{b}_1$ and $\mathbf{b}_2$ are the reciprocal-lattice vectors, $K(K')$ and $K_1(K_1')$ are the two sets of Dirac points. (c) The electronic dispersion for $t_{12}=t_{23}=t_{31}=1.0$.

$$f(\mathbf{k}) = 8\cos(k_x/2)\cos(k_x/4+\sqrt{3}k_y/4)\cos(k_x/4-\sqrt{3}k_y/4),$$

and the energy band structure is shown in Fig. 1(c). The two dispersive bands E^+ and E^- contact at the corners of the first Brillouin zone (BZ) (named as Dirac points) such as $K=(4\pi/3,0)$ and $K'=(2\pi/3,2\pi/\sqrt{3})$, etc. Near the Dirac points, electrons behave as Dirac fermions with the approximate dispersion,

$$E_\pm = -t \pm v_F|\mathbf{q}| + O[(q/K)^2], \tag{4}$$

and $v_F=3\sqrt{2}t/4$ is the Fermi velocity. Thus, except for an additional flat band E_3, the two dispersive energy bands are similar to those in graphene. As a result, an unconventional QHE as that found in graphene is expected on the isotropic kagome lattice around the Fermi level $\mu=-t$ (corresponding to the electron filling 1/3).

We now turn to the numerical investigation of the QHE on the anisotropic kagome lattice. In a perpendicular magnetic field, the tight-binding Hamiltonian is changed into,

$$\hat{H} = -\sum_{\langle ij\rangle,\sigma}(t_{ij}e^{i\alpha_{ij}}\hat{c}^\dagger_{i\sigma}\hat{c}_{j\sigma} + \text{H.C.}). \tag{5}$$

Equation (5) will be diagonalized numerically on a finite lattice with size $N=3\times L_1\times L_2$ (factor three counts the three sites in each unit cell). The magnetic flux per triangular is chosen to be $\phi=\Sigma_\Delta\alpha_{ij}=\frac{2\pi}{M}$, with M as an integer, then the total flux $\Phi=\frac{16\pi N}{3M}$ through the lattice is taken to satisfy the periodic boundary condition. Typically, $N=3\times320\times320$ and $\phi=\frac{2\pi}{2560}$ are used in numerical calculations. After the diagonalization, the Hall conductivity σ_{xy} is calculated with Kubo formula

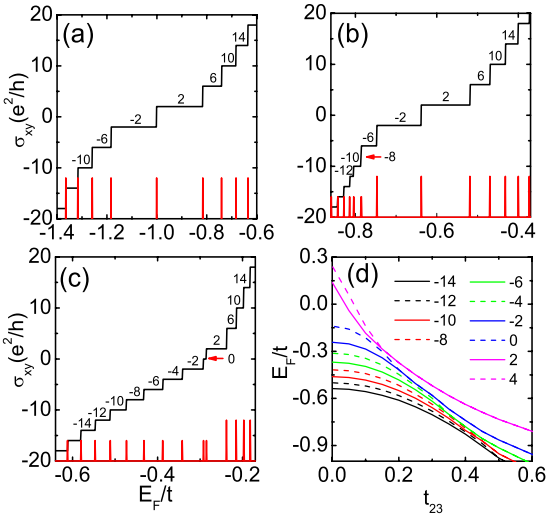

FIG. 2. (Color online) (a)–(c) Hall conductivities vs Fermi energy for different t_{23} and the corresponding DOS denoted by red vertical lines. (a), (b), and (c) correspond to $t_{23}=1.0$, 0.4, and 0.15, respectively. The red horizontal arrows in (b) and (c) indicate the transition point from $g_s=4$ to $g_s=2$. (d) Phase diagram showing the gradual splitting of the Hall plateaus with the decrease in t_{23}. The solid lines denote the original plateaus and the dashed lines denote the new plateaus induced by the anisotropy. The numbers on each plateau and in panel (d) denote ν in $\sigma_{xy}=\nu e^2/h$.

$$\sigma_{xy} = A\sum_{\varepsilon_\alpha<E_F}\sum_{\varepsilon_\beta>E_F}\frac{\langle\alpha|v_x|\beta\rangle\langle\beta|v_y|\alpha\rangle-\langle\alpha|v_y|\beta\rangle\langle\beta|v_x|\alpha\rangle}{(\varepsilon_\alpha-\varepsilon_\beta)^2}, \tag{6}$$

where $A=i2e^2/S\hbar$ with S being the area of the system, v is the velocity, ε_α and ε_β are the corresponding eigenvalues of the eigenstates $|\alpha\rangle$ and $|\beta\rangle$. In the following, the hopping integrals $t_{12}=t_{31}=1.0$ are used as the energy unit and t_{23} to account for the anisotropy.

In Fig. 2, the Hall conductivity $\sigma_{xy}=\nu e^2/h$ and the electron density of states (DOS) are plotted for the different t_{23}. For the isotropic case with $t_{23}=1.0$, the Hall plateaus satisfy the unconventional quantization rule $\nu=(n+1/2)g_s$ with a degeneracy factor $g_s=4$ for each Landau level to count two spin components and two Dirac points. The 1/2 shift in the Hall plateaus is due to a nonzero Berry phase around Dirac points,[16] or can be explained simply as arising from the existence of a zero mode as seen from the DOS shown in Fig. 2(a). This numerical result is consistent with the above analytical calculation, showing that the QHE on the isotropic kagome lattice exhibits the same behavior as that in graphene.

Decreasing t_{23} to introduce the anisotropy in the hopping integral, one will find that the steps in Hall conductivity split at the mid point gradually, as shown in Figs. 2(b) and 2(c). Concomitant with the splitting, a new Hall plateau emerges between every two Hall plateaus and the degeneracy factor g_s changes from four to two. Basically, one might expect that, upon the introduction of the anisotropy, the rotational symmetry of the isotropic kagome lattice will be broken, and consequently the degenerate energy levels will be separated.

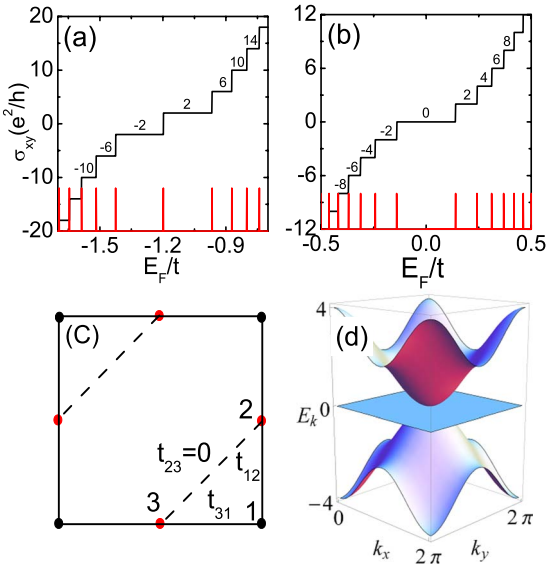

FIG. 3. (Color online) (a) and (b) are the Hall conductivities together with the DOS for $t_{23}=2.0$ and $t_{23}=0$, respectively. (c) The square lattice, which is equivalent topologically to the kagome lattice for $t_{23}=0$, and its energy bands in (d).

Indeed, at the energy levels, where the step splitting in Hall conductivity occurs, the peak of DOS (denoted as red vertical lines in Fig. 2) is split into two adjacent peaks with half a previous height. However, two nontrivial characters exhibit here. One is that the splitting does not happen as a whole simultaneously, but gradually from low energies to high energies with the decrease in t_{23} (corresponding to the enhancement of the anisotropy). Moreover, whenever a splitting occurs, a new Hall plateau emerges. But, the next splitting does not happen in succession with the further decrease in t_{23}, instead the emerging plateau will grow first until it satisfies the new quantization rules for the Landau Level, which will be addressed in the following. This process can also be clearly seen from the peak splitting in DOS. In this way, the QHE on the anisotropic kagome lattice exhibits a sequent quantum phase transition from low to high energies, and the phase diagram is presented in Fig. 2(d). Second, in the case of $t_{23}>1$, we find that the peaks in DOS do not split at any energy level in the reasonable parameter regime. For example, at least for the largest anisotropy $t_{23}=2$ considered here [see Fig. 3(a)], the QHE shows the same behavior to the isotropic case.

The quantum phase transition demonstrated above is in contrast to that on the honeycomb lattice (graphene),[12–15] where the unconventional QHE changes into the conventional QHE with $\sigma_{xy}=2ne^2/h$ in the strong t_{23} ($t_{23}>1$) regime, while no phase transition occurs for the weak t_{23} ($t_{23}<1$) regime. In addition, the phase transition on the anisotropic honeycomb lattice starts symmetrically from both the low and high energies, and gradually approaches the zero-energy level, so that it exhibits a particle-hole symmetry.

Next, let us study the character manifested by the new phase emerging in the quantum phase transition. This is accessible easily in the limit $t_{23}=0$, where the kagome lattice is topologically equivalent to the lattice in Fig. 3(c) with only

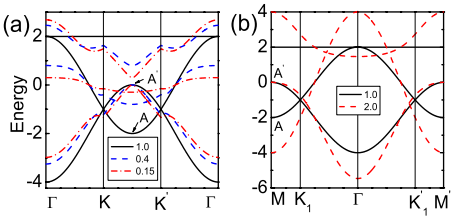

FIG. 4. (Color online) The energy bands for different t_{23}. (a) In weak t_{23} regime and (b) in strong t_{23} regime. For the momentum directions in (a) and (b), see Fig. 1(b) for illustration. The black, blue, and red lines in panel (a) correspond to $t_{23}=1$, 0.4, and 0.15. The red dashed lines in panel (b) is for $t_{23}=2.0$.

the nearest-neighbor hoppings. The three energy bands on this lattice can be found as, $E_{\pm}=\pm 2t\sqrt{\cos^2(k_x/2)+\cos^2(k_y/2)}$ and $E_3=0$, as shown in Fig. 3(d). Around $\mathbf{K}_0=(\pi,\pi)$, the bands $E_{\pm}$ have the linear dispersion $E_{\pm}(\mathbf{q})=\pm v_F|\mathbf{q}|$ with $v_F=\sqrt{2}t$. Because the flat band E_3 crosses the $\mathbf{K}_0$ point, the electrons do not behave as massless Dirac fermions. In this respect, the Hall conductivity shows a conventional behavior $\sigma_{xy}=2ne^2/h$. However, the LL spectrum exhibits a different form. This can be obtained analytically by solving the low-energy Hamiltonian of the system, as given by

$$\hat{H}=\frac{v_F}{\sqrt{2}}\begin{pmatrix}0 & \hat{p}_x & \hat{p}_y\\ \hat{p}_x^{\dagger} & 0 & 0\\ \hat{p}_y^{\dagger} & 0 & 0\end{pmatrix}, \tag{7}$$

under a magnetic field $\mathbf{B}$ [correspond to replace the momentum operator $\hat{\mathbf{p}}$ by $\hat{\mathbf{p}}+e\mathbf{A}$ with $\mathbf{A}=B(-y,0)$]. The result is,

$$E(n)=\pm v_F\sqrt{(n+1/2)\hbar Be},\quad n=1,2,3,\cdots. \tag{8}$$

This LL spectrum leads to a distinct distribution of Hall plateaus, as shown in Fig. 3(b). It is quite different from that in free-fermion systems exhibiting equidistant Hall plateaus $(n+1/2)\hbar\omega_c$ and in bilayer graphenes with almost equidistant plateaus $\sqrt{n(n-1)}\hbar\omega_c$.[9,10] It is also different from that in graphenes with $v_F\sqrt{2n\hbar Be}$.[8] Though this difference is hard to distinguish numerically, the two differ remarkably in the Hall conductivity σ_{xy} as addressed above. These comparisons suggest that the energy spectrum of the QHE demonstrated here has no known analogs and may be distinguished on the basis of the QHE measurements.

To understand the property of the quantum phase transition, we show in Fig. 4 the evolution of the energy band with the hopping integral t_{23} along two high symmetrical directions. First, we point out that the unconventional QHE is found numerically to be limited to a finite-energy range (not shown here), which is the region from A to A' (points of the van Hove singularity) in the dispersions shown in Fig. 4. Outside this region, the QHE will exhibit a conventional behavior in Hall conductivity. For $t_{23}<1$ [Fig. 4(a)], the two Dirac points, which are at K and K' points in the isotropic case, approach each other along the K-K' direction with the decrease in t_{23}. Interestingly, in this process, the energy band around the A point is suppressed and lifted upward gradually, while that around the A' point is not changed. As a result, the

low-energy part will be excluded out of the unconventional regime. Therefore, the conventional Hall conductivity emerges first at these energy levels. On the other hand, for $t_{23}>1$ [Fig. 4(b)] the two Dirac points approach each other along the K_1-Γ-K_1' direction. Different from the case of $t_{23}<1$, the energy band around A now is shifted downward with the increase in t_{23}, so that the energy region exhibiting the unconventional Hall conductivity is enlarged. Therefore, no quantum phase transition is observed in the energy region considered.

Finally, let us give a few comments on the possible experimental realization of our theoretical prediction. The anisotropy of the hopping integral can be realized by the monoclinic lattice distortion, such as in $Cu_{(3)}V_2O_7(OH)_2\cdot 2H_2O$,[17] or by the difference in orbital characters on the atomic sites due to the Jahn-Teller effect, such as in $Cs_2Cu_3CeF_{12}$.[18] The kagome lattice has been proposed to be realized by implementing an optical lattice for ultracold atoms.[19–21] In this regard, the ability to conveniently control the physical parameters facilitates the realization of the anisotropy. It is also worth mentioning that the 2D lattice in the limit $t_{23}=0$ as shown in Fig. 3(c) may provide an interesting model system for experimental investigation on the special quantum dynamics demonstrated above.

In summary, we have studied the quantum Hall effect on the anisotropic kagome lattice. The anisotropy is introduced by assuming one of the hopping integrals t_{23} taking a different value. In the weak t_{23} ($t_{23}<t_{12}$) regime, we find an interesting quantum phase, in which the QHE exhibits a special-energy spectrum given by $E(n)=\pm v_F\sqrt{(n+1/2)\hbar Be}$, though its Hall conductivity $\sigma_{xy}=2ne^2/h$ is conventional. This phase evolves from the unconventional QHE with $\sigma_{xy}=4(n+1/2)e^2/h$ via a quantum phase transition, which occurs successively from low to high energies with the decrease in the hopping integral. The quantum phase transition is absent in the strong t_{23} regime.

ACKNOWLEDGMENTS

We acknowledge valuable discussions with D. H. Lee and X. G. Wen. This work was supported by the National Natural Science Foundation of China (Grants No. 10525415 and No. 10874066), the Ministry of Science and Technology of China (973 project Grants No. 2006CB601002,2006CB921800, No. 2007CB925104, and No. 2009CB929504).

*jxli@nju.edu.cn

[1] R. E. Prange and S. M. Girvin, *The Quantum Hall Effect* (Springer, New York, 1990).
[2] K. S. Novoselov, A. K. Geim, S. V. Morozov, D. Jiang, M. I. Katsnelson, I. V. Grigorieva, S. V. Dubonos, and A. A. Firsov, Nature (London) **438**, 197 (2005).
[3] Y. Zhang, Y.-W. Tan, H. L. Stormer, and P. Kim, Nature (London) **438**, 201 (2005).
[4] F. D. M. Haldane, Phys. Rev. Lett. **61**, 2015 (1988).
[5] Y. Zheng and T. Ando, Phys. Rev. B **65**, 245420 (2002).
[6] V. P. Gusynin and S. G. Sharapov, Phys. Rev. Lett. **95**, 146801 (2005).
[7] D. N. Sheng, L. Sheng, and Z. Y. Weng, Phys. Rev. B **73**, 233406 (2006).
[8] A. H. Castro Neto, F. Guinea, N. M. R. Peres, K. S. Novoselov, and A. K. Geim, Rev. Mod. Phys. **81**, 109 (2009).
[9] K. S. Novoselov, E. Mccann, S. V. Morozov, V. I. Falko, M. I. Katsnelson, U. Zeitler, D. Jiang, F. Schedin, and A. K. Geim, Nat. Phys. **2**, 177 (2006).
[10] E. McCann and V. I. Falko, Phys. Rev. Lett. **96**, 086805 (2006).
[11] A. Mielke, J. Phys. A **24**, L73 (1991).
[12] M. Sato, D. Tobe, and M. Kohmoto, Phys. Rev. B **78**, 235322 (2008).
[13] Y. Hasegawa, R. Konno, H. Nakano, and M. Kohmoto, Phys. Rev. B **74**, 033413 (2006).
[14] P. Dietl, F. Piéchon, and G. Montambaux, Phys. Rev. Lett. **100**, 236405 (2008).
[15] M. Kohmoto and Y. Hasegawa, Phys. Rev. B **76**, 205402 (2007).
[16] G. P. Mikitik and Yu. V. Sharlai, Phys. Rev. Lett. **82**, 2147 (1999).
[17] F. Bert, D. Bono, P. Mendels, F. Ladieu, F. Duc, J.-C. Trombe, and P. Millet, Phys. Rev. Lett. **95**, 087203 (2005).
[18] T. Amemiya, M. Yano, K. Morita, I. Umegaki, T. Ono, H. Tanaka, K. Fujii, and H. Uekusa, Phys. Rev. B **80**, 100406 (2009).
[19] L. Santos, M. A. Baranov, J. I. Cirac, H.-U. Everts, H. Fehrmann, and M. Lewenstein, Phys. Rev. Lett. **93**, 030601 (2004).
[20] J. Ruostekoski, Phys. Rev. Lett. **103**, 080406 (2009).
[21] B. Damski, H. Fehrmann, H.-U. Everts, M. Baranov, L. Santos, and M. Lewenstein, Phys. Rev. A **72**, 053612 (2005).